Supplementary information

Cobalt-ferrite functionalized graphitic carbon nitride ($CoFe_2O_4$@g-C_3N_4) nanoconfined catalytic membrane for efficient water purification: Performance and mechanism

Wei Zhang[a,b,c], Shaoze Zhang[d], Zhen Chen[e], and Zhenghua Zhang[a,b,c*]

[a]Membrane & Nanotechnology-Enabled Water Treatment Center, Institute of Environment and Ecology, Tsinghua Shenzhen International Graduate School, Tsinghua University, Shenzhen 518055, Guangdong, China

[b]Guangdong Provincial Engineering Research Center for Urban Water Recycling and Environmental Safety, Tsinghua-Shenzhen International Graduate School, Tsinghua University, Shenzhen 518055, Guangdong, China

[c]School of Environment, Tsinghua University, Beijing 100084, China

[d]National Engineering Research Center for Vacuum Metallurgy, Engineering Laboratory for Advanced Battery and Materials of Yunnan Province, Kunming University of Science and Technology, Kunming 650093, Yunnan province, China

[e]Institute of Material, Tsinghua Shenzhen International Graduate School, Tsinghua University, Shenzhen 518055, Guangdong, China.

Journal of Materials Chemistry A

Submitted June 2023

*Corresponding author: zhenghua.zhang@sz.tsinghua.edu.cn (Z. Zhang)

Text S1. Chemicals

Ranitidine hydrochloride (> 98%) was received from Tokyo Chemical Industry Co. Ltd. Urea, tetracycline (TC), carbamazepine (CBZ), sulfamethoxazole (SMZ) were purchased from Shanghai Yuanye Bio-Technology Co., Ltd. Iron(II) sulfate heptahydrate ($FeSO_4 \cdot 7H_2O$) was supplied by Sinopharm Chemical Reagent Co., Ltd. Cobalt nitrate hexahydrate ($Co(NO_3)_2 \cdot 6H_2O$) was purchased from Meryer Co., Ltd. L-Histidine base (L-HIS) was purchased from Biofroxx GmbH. 2,2,6,6-Tetramenthyl-4-piperidone hydrochloride (TEMP, ≥ 99.0%) was obtained from Dojindo Co., Ltd. Phenol was supplied by ANPEL Laboratory Technologies (Shanghai) Inc. PMS ($KHSO_5$, ≥ 99.0%), oxalic acid dihydrate ($H_2C_2O_4 \cdot 2H_2O$), methyl orange (MO, IND), Tert-butyl alcohol (TBA, ≥ 99.5%), 5,5-dimethyl-1-pyrroline (DMPO, ≥ 99.0%) and methanol (≥ 99.5%) were purchased from Aladdin Industrial Corporation. All solutions were prepared with ultrapure water produced by a Milli-Q system.

Text S2. Characterizations of $CoFe_2O_4$@g-C_3N_4 membranes

Scanning electron microscopy (SEM, TESCAN MIRA LMS, TESCAN, Czech) was used to observe the morphology of $CoFe_2O_4$@g-C_3N_4 NS, membrane surface, and membrane cross-section. Transmission electron microscopy (TEM; FEI Tecnai F20, FEI, Netherlands) was used to examine the microstructure of the $CoFe_2O_4$@g-C_3N_4 NS. X-ray diffraction (XRD; SmartLab SE, Rigaku, Japan) was adopted to determine the crystal structure of the $CoFe_2O_4$@g-C_3N_4 NS and the $CoFe_2O_4$@g-C_3N_4 membrane. Fourier transform infrared (FTIR) spectroscopy (Nicolet iS20, Thermo Fisher Scientific, America) was used to detect the chemical bonds in g-C_3N_4 NS and $CoFe_2O_4$@g-C_3N_4 NS. The chemical states of the elements in the fresh $CoFe_2O_4$@g-C_3N_4 membrane and the used $CoFe_2O_4$@g-C_3N_4 membrane were determined by X-ray photoelectron spectroscopy (XPS; Thermo Scientific K-Alpha, Thermo Fisher Scientific, America). The thickness of the $CoFe_2O_4$@g-C_3N_4 NS was measured by atomic force microscopy (AFM, Bruker Dimension Icon, Bruker, Germany). The pore size and specific surface area of the $CoFe_2O_4$@g-C_3N_4

membrane were measured by nitrogen adsorption-desorption isotherms using the Brunauer-Emmett-Teller (BET) theory (ASAP 2460, Micromeritics, USA). Total organic carbon (TOC) analyzer (TOC-V_{CPH}, Shimadzu, Japan) was used to measure the mineralization efficiency of pollutants. The ROS generated during the catalytic process were identified using electron paramagnetic resonance (EPR) spectroscopy (MS-5000, Bruker, Germany). Inductively coupled plasma-mass spectrometry (ICP-MS, Agilent 720ES, Agilent, USA) was used to quantify cobalt and iron dissolved. The instrument parameters are listed in Table S1. Liquid chromatography-mass spectrometry (LC-MS, 1290UPLC-6550QTOF, Agilent, USA) was used to detect degradation intermediates, and the operating conditions were listed in Table S2.

Text S3. DFT calculations

All the periodical calculations were carried out by the Vienna Ab initio Simulation Package (VASP) software [1-4]. The Perdew-Burke-Ernzerhof (PBE) exchange-correlation functions [5] with a projector-augmented wave (PAW) scheme [6] was implied to describe the ion-electron exchange-correlation. The DFT-D3 [7], including Becke-Johnson damping [8] was used to correct the dispersion. The energy cutoff for the plane-wave expansion was setup to the value of 450 eV. The Brillouin zone integration was generated according to the Monkhorst-Pack method [9] using a Gamma centered 2 × 2 × 1 *k*-point mesh. All structures were relaxed until the energy changed below 1×10^{-5} eV, and the forces on each atom less than 0.01 eV/Å.

To model the $CoFe_2O_4$@g-C_3N_4 substrate, a heterojunction contains the plane of $CoFe_2O_4$ (111) and g-C_3N_4 (001) was constructed. The adsorption energy (E_{ads}) was calculated as:

$$E_{ads} = E_{system} - E_{surface} - E_{PMS} \tag{1}$$

where the E_{system} is the energy of the optimized PMS/$CoFe_2O_4$@g-C_3N_4 system; $E_{surface}$ is the energy of the bare $CoFe_2O_4$@g-C_3N_4 heterojunction; E_{PMS} is the energy of an optimized PMS molecule within a 30 × 30 × 30 box.

To illustrate the PMS dissociation process, the transition states were located utilizing the climbing Nudged Elastic Band (CINEB) method implemented in VASP-

VTST code [10]. After the CINEB calculations, the frequency calculations were performed with a numerical algorithm and atomic displacement of 0.015Å. A true transition state from CINEB calculations was confirmed by a single negative frequency. The free energy corrections were accomplished with the VASPKIT program [11] at the temperature of 298.15K.

The electron density difference (EDD) was defined as:

$$\Delta\rho(r) = \rho_{system}(r) - \rho_{g-C_3N_4}(r) - \rho_{CoFe_2O_4}(r) - \rho_{SO_4}(r) - \rho_{OH}(r) \quad (2)$$

where ρ_{system}, $\rho_{g\text{-}C3N4}$, $\rho_{CoFe2O4}$, ρ_{SO4}, and ρ_{OH} are the electronic densities of the PMS/ $CoFe_2O_4$@g-C_3N_4 system, $CoFe_2O_4$, g-C_3N_4, SO_4 and OH species, respectively.

Text S4. Crystal plane spacing calculation

The crystal plane spacing was calculated using the Bragg equation:

$$d = \frac{n\lambda}{2sin\theta} \quad (3)$$

where d (nm) represents the crystal plane spacing; n is the diffraction order (value is 1); λ (nm) is the wavelength (0.1542 nm) ; θ (°) is the diffraction half-angle.

Text S5. Membrane flux calculation

The membrane water flux J ($L \cdot m^{-2} \cdot h^{-1}$) through the $CoFe_2O_4$@g-C_3N_4 membrane was calculated using Equation (4):

$$J = \frac{V}{A \times T} \quad (4)$$

where J is the water flux at 1 bar; V (L) represents the membrane-permeated solution volume; A (m^2) represents the effective membrane filtration surface area (1.766 cm^2); T (h) is the filtration time.

Text S6. Determination of PMS decomposition efficiency

Firstly, a test solution containing 100 g/L KI and 5 g/L $NaHCO_3$ was prepared. Then, 0.2 mL sample and 20 mL test solution were fully mixed and placed for more than 30 min followed by the UV absorbance measurement at 352 nm. The PMS decomposition efficiency, D (%), was calculated using Equation (5):

$$D = \frac{A_0 - A_t}{A_0} \times 100\% \tag{5}$$

where A_0 is the absorbance of the original PMS test solution, and A_t is the absorbance of the sample solution at the specified time point.

Text S7. Membrane retention time calculation

The retention time (r_m, ms) in the $CoFe_2O_4$@g-C_3N_4 membrane was calculated as follows:

$$r_m = \frac{V \times M}{J \times A} \tag{6}$$

where V ($cm^3 \cdot g^{-1}$) represents the specific pore volume of the $CoFe_2O_4$@g-C_3N_4 membrane, M (g) is the total mass of the $CoFe_2O_4$@g-C_3N_4 membrane, J ($L \cdot m^{-2} \cdot h^{-1}$) represents the membrane water flux, A (m^2) is the effective membrane filtration surface area.

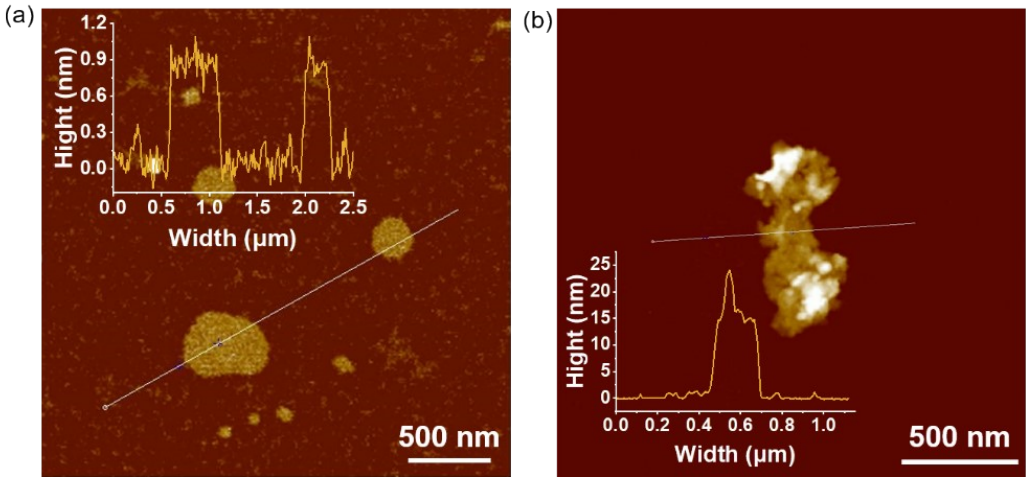

Figure S1. The thickness of g-C_3N_4 NS (a) and $CoFe_2O_4$@g-C_3N_4 NS (b) measured by AFM.

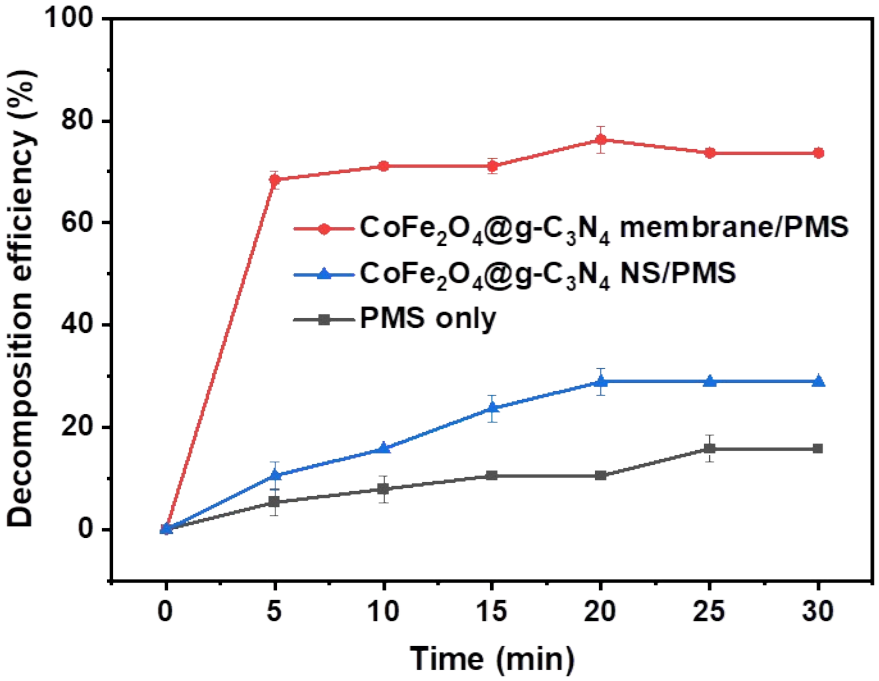

Figure S2. Decomposition efficiency of PMS in different systems.

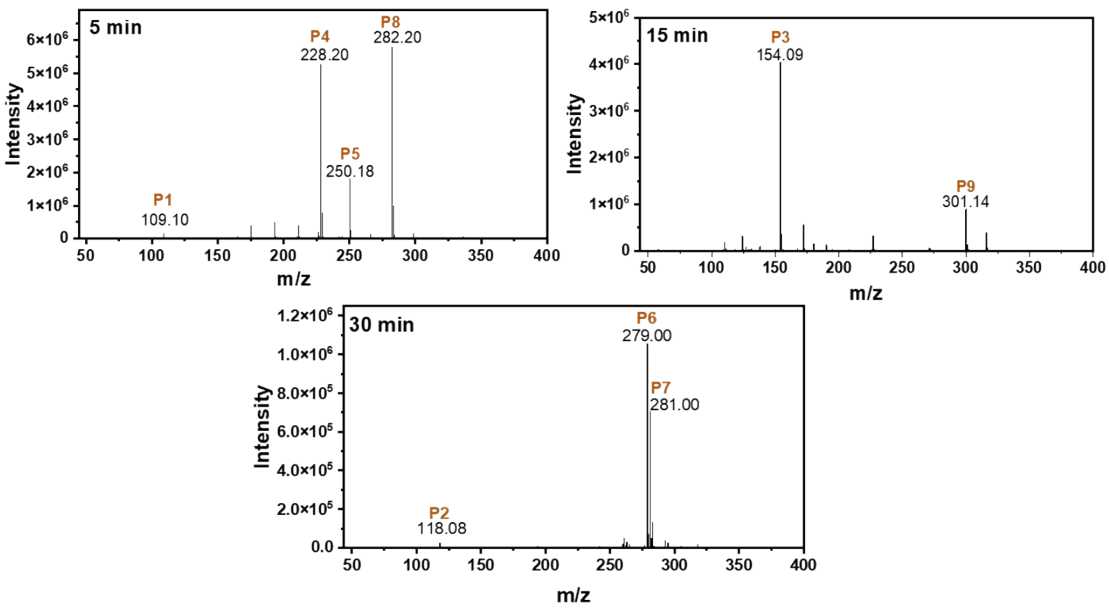

Figure S3. Spectra of ranitidine degradation intermediates by the $CoFe_2O_4$@g-C_3N_4 membrane/PMS system at different reaction times: 5 min, 15 min and 30min.

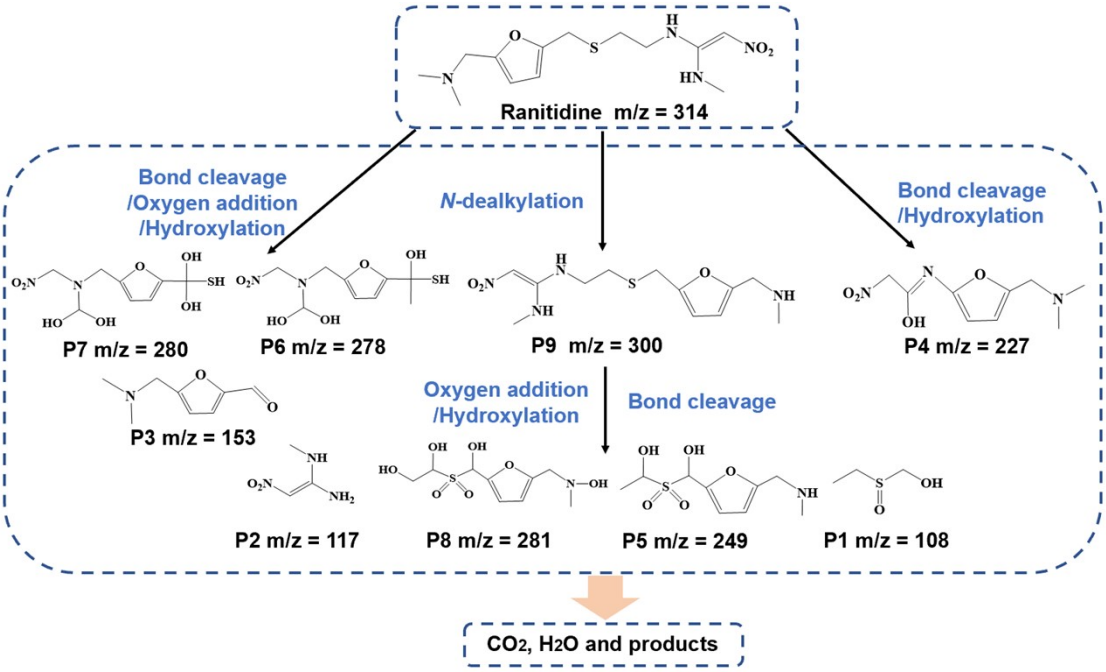

Figure S4. Possible degradation pathways of ranitidine in the $CoFe_2O_4$@g-C_3N_4 membrane/PMS system.

Table S1. Test results and instrument parameters of ICP-MS.

Instrument parameters	RF Power	1.50 KW	Omega Lens	10.1 V
	RF Matching	1.80 V	Cell Entrance	-45 V
	Auxiliary flow	1.50 L/min	Deflect	3.8 V
	Carrier Gas	1.10 L/min	Cell Exit	-62 V
	Omega Bias	-105 V	Plate Bias	-60 V
Test results	Element	Co	Concentration	24.79 μg/L
		Fe	Concentration	10.24 μg/L

Table S2. Operating conditions of LC-MS.

LC operating conditions		**MS operating conditions**	
Eluent A	0.1% Formic acid	Detection mode	ESI+
Eluent B	Methanol	Gas temperrature	350℃
Chromatographic column	Waters BEH C18 2.1×100 mm 1.7 μm	Mass spectrum scanning range	30-1000 m/z
Sample injection	5 μL	Gas flow rate	12 L/min
Liquid flow rate	0.3 mL/min	Voltage	4000 V

Table S3. Comparison of first-order rate constants of ranitidine removal in different systems.

Methods	Materials	Ranitidine concentration (mg/L)	Removal efficiency	Reaction time	Catalyst dosage	k (min^{-1})	Ref
Photocatalysis	PMOFs	38	93.1%	120 min	100 mg/L	0.01833	12
Photocatalysis	Fe^{2+}/PS	9	95%	60 min	50 mg/L	0.05	13
Photocatalysis	Fe_3O_4/GE/SCN	1	100%	40 min	1 g/L	0.077	14
Photocatalysis	MXene-Ti_3C_2/MoS_2	10	88.4%	60 min	1 g/L	0.0315	15
Photocatalysis	MXene-Ti_3C_2	10	18.4%	60 min	1 g/L	0.0032	15
Photocatalysis	Degussa P25 nanoparticles	3	--	120 min	--	0.011	16
Photocatalysis	TiO_2-nanofiber film	3	--	129 min	--	0.0080	16
Heterogeneous catalysis	OM-Co_3O_4	10	99.2%	7 min	0.025 g/L	0.719	17

Heterogeneous catalysis	BN- Co_3O_4 NC	10	99.6%	10 min	0.03 g/L	0.682	18
Heterogeneous catalysis	Co_3O_4 NS	5	47.2%	30 min	0.02 g/L	0.021	19
Heterogeneous catalysis	Co-Cu ONS	5	100%	60 s	0.017 g/L	4.2	20
Membrane-based nanoconfinement catalysis	Co_3O_4 membrane	5	100%	385 ms	0.7 mg/cm^2	600	19
Membrane-based nanoconfinement catalysis	Co-Cu ONS membrane	5	100%	85.7 ms	0.4 mg/cm^2	3180	20
Membrane-based nanoconfinement catalysis	Co@g-C_3N_4 membrane	5	100%	33 ms	0.75 mg/cm^2	4800	21
Heterogeneous catalysis	$CoFe_2O_4$@g-C_3N_4 NS	5	49.4%	30 min	0.02 g/L	0.0229	This work
Membrane-based nanoconfinement catalysis	$CoFe_2O_4$@g-C_3N_4 membrane	5	100%	54.6 ms	0.5 mg/cm^2	5280	This work

Table S4. XPS of the fresh and the used membranes.

Element	Bond type	Fresh membrane			Used membrane		
		E/ev	A	at/%	E/ev	A	at/%
Co 2*p*	≡Co(II)	781.1	9419.98	24.05	781.4	33199.42	15.28
		785.5	7461.12	19.06	785.5	65204.36	29.90
		794.9	2835.08	7.33	795.5	11318.49	5.32
		801.8	5222.52	13.49	802.0	20009.56	8.97
	≡Co(III)	778.6	11458.29	29.33	779.0	72852.86	33.22
		793.6	2670.55	6.74	794.0	16303.79	7.31
Fe 2*p*	≡Fe(II)	709.2	20222.68	32.26	709.1	95364.95	22.03
		715.0	7287.71	11.61	714.9	43233.69	10.04
		722.4	6443.34	10.32	722.6	72451.52	16.96
		729.4	2304.92	3.55	729.1	16659.34	3.92
	≡Fe(III)	711.5	10483.17	16.77	711.36	100769.19	23.33
		718.9	6082.94	9.68	718.2	46835.25	10.92
		724.8	7411.74	11.94	725.4	38183.34	8.96
		732.9	2423.57	3.87	732.5	16193.19	3.83

Table S5. Intermediate products of ranitidine degradation.

Compounds	Molecular mass	Experimental mass	Structure
Ranitidine	314	315.0	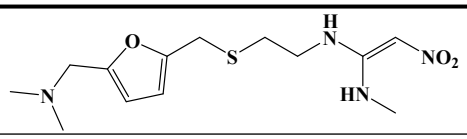
P1	108	109.10	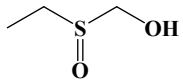
P2	117	118.08	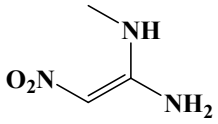
P3	153	154.09	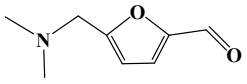
P4	227	228.20	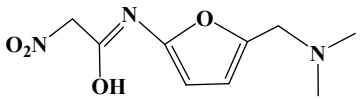
P5	249	250.18	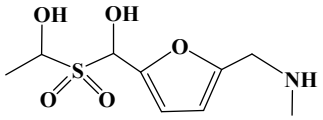
P6	278	279.00	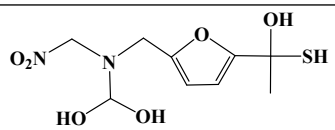
P7	280	281.00	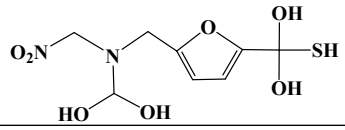
P8	281	282.21	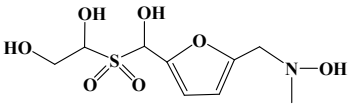
P9	300	301.14	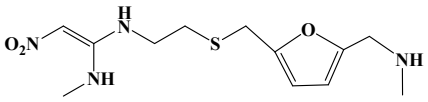

References

[1] G. Kresse, J. Hafner, Ab initio molecular dynamics for liquid metals, Phys. Rev. B. 47 (1993) 558–561. DOI:10.1103/PhysRevB.47.558.

[2] G. Kresse, J. Hafner, Ab initio molecular-dynamics simulation of the liquid-metal-

-amorphous-semiconductor transition in germanium, Phys. Rev. B. 49 (1994) 14251–14269. DOI:10.1103/PhysRevB.49.14251.

[3] G. Kresse, J. Furthmüller, Efficiency of ab-initio total energy calculations for metals and semiconductors using a plane-wave basis set, Comput. Mater. Sci. 6 (1996) 15–50. DOI:10.1016/0927-0256(96)00008-0.

[4] G. Kresse, J. Furthmüller, Efficient iterative schemes for ab initio total-energy calculations using a plane-wave basis set, Phys. Rev. B. 54 (1996) 11169–11186. DOI:10.1103/PhysRevB.54.11169.

[5] J.P. Perdew, K. Burke, M. Ernzerhof, Generalized Gradient Approximation Made Simple, Phys. Rev. Lett. 77 (1996) 3865–3868. DOI:10.1103/PhysRevLett.77.3865.

[6] G. Kresse, D. Joubert, From ultrasoft pseudopotentials to the projector augmented-wave method, Phys. Rev. B. 59 (1999) 1758–1775. DOI:10.1103/PhysRevB.59.1758.

[7] S. Grimme, J. Antony, S. Ehrlich, H. Krieg, A consistent and accurate ab initio parametrization of density functional dispersion correction (DFT-D) for the 94 elements H-Pu, J. Chem. Phys. 132 (2010) 154104. DOI:10.1063/1.3382344.

[8] A.D. Becke, E.R. Johnson, Exchange-hole dipole moment and the dispersion interaction, J. Chem. Phys. 122 (2005) 154104. DOI:10.1063/1.1884601.

[9] H.J. Monkhorst, J.D. Pack, Special points for Brillouin-zone integrations, Phys. Rev. B Condens. Matter. 13 (1976) 5188–5192. DOI:10.1103/PhysRevB.13.5188.

[10] G. Henkelman, B. Uberuaga, H. Jónsson, A climbing image nudged elastic band method for finding saddle points and minimum energy paths, (2000). DOI:10.1063/1.1329672.

[11] V. Wang, N. Xu, J.C. Liu, G. Tang, W. Geng, VASPKIT: A user-friendly interface facilitating high-throughput computing and analysis using VASP code, Comput Phys Commun. (2021). DOI:10.1016/j.cpc.2021.108033.

[12] J. Li, Y. Zhao, X. Wang, T. Wang, X. Hou, Rapid microwave synthesis of PCN-134-2D for singlet oxygen based-oxidative degradation of ranitidine under visible light: Mechanism and toxicity assessment, Chem. Eng. J. 443 (2022) 136424. DOI:

10.1016/j.cej.2022.136424.

[13] S. Naim, A. Ghauch, Ranitidine abatement in chemically activated persulfate systems: Assessment of industrial iron waste for sustainable applications, Chem. Eng. J. 288 (2016) 276–288. DOI: 10.1016/j.cej.2015.11.101.

[14] L. Wang, Q. Sun, Y. Dou, Z. Zhang, T. Yan, Y. Li, Fabricating a novel ternary recyclable Fe_3O_4/graphene/sulfur-doped g-C_3N_4 composite catalyst for enhanced removal of ranitidine under visible-light irradiation and reducing of its N-nitrosodimethylamine formation potential, J. Hazard. Mater. 413 (2021) 125288. DOI: 10.1016/j.jhazmat.2021.125288.

[15] X. Zou, X. Zhao, J. Zhang, W. Lv, L. Qiu, Z. Zhang, Photocatalytic degradation of ranitidine and reduction of nitrosamine dimethylamine formation potential over MXene–Ti_3C_2/MoS_2 under visible light irradiation, J. Hazard. Mater. 413 (2021) 125424. DOI: 10.1016/j.jhazmat.2021.125424.

[16] K.J. Choi, S.W. Hong, Preparation of TiO_2 nanofibers immobilized on quartz substrate by electrospinning for photocatalytic degradation of ranitidine, Res Chem Intermed. 38 (2012) 1161–1169. DOI: 10.1007/s11164-011-0455-z.

[17] Y. Ma, H. Wang, X. Lv, D. Xiong, H. Xie, Z. Zhang, Three-dimensional ordered mesoporous Co_3O_4/peroxymonosulfate triggered nanoconfined heterogeneous catalysis for rapid removal of ranitidine in aqueous solution, Chemical Engineering Journal. 443 (2022) 136495. DOI:10.1016/j.cej.2022.136495.

[18] Y. Ma, B. Ji, X. Lv, D. Xiong, X. Zhao, H. Xie, Z. Zhang, Confined heterogeneous catalysis by boron nitride-Co_3O_4 nanosheet cluster for peroxymonosulfate oxidation toward ranitidine removal, Chemical Engineering Journal. 435 (2022) 135126. DOI:10.1016/j.cej.2022.135126.

[19] Z. Wang, C. Meng, W. Zhang, S. Zhang, B. Yang, Z. Zhang, Honeycomb-like holey Co_3O_4 membrane triggered peroxymonosulfate activation for rapid degradation of organic contaminants, Science of The Total Environment. 814 (2022) 152698. DOI:10.1016/j.scitotenv.2021.152698.

[20] C. Meng, Z. Wang, W. Zhang, L. Cui, B. Yang, H. Xie, Z. Zhang, Laminar membranes assembled by ultrathin cobalt-copper oxide nanosheets for

nanoconfined catalytic degradation of contaminants, Chemical Engineering Journal. 449 (2022) 137811. DOI:10.1016/j.cej.2022.137811.

[21] W. Zhang, S. Zhang, C. Meng, Z. Zhang, Nanoconfined catalytic membranes assembled by cobalt-functionalized graphitic carbon nitride nanosheets for rapid degradation of pollutants, Applied Catalysis B: Environmental. 322 (2023) 122098. DOI:10.1016/j.apcatb.2022.122098.